Carbon 99 (2016) 416–422

Contents lists available at ScienceDirect

Carbon

journal homepage: www.elsevier.com/locate/carbon

Acoustic surface phonons of graphene on Ni(111)

Amjad al Taleb [a], Gloria Anemone [a], Daniel Farías [a, b, c, *], Rodolfo Miranda [a, b, c, d]

[a] Departamento de Física de la Materia Condensada, Universidad Autónoma de Madrid, 28049 Madrid, Spain
[b] Instituto "Nicolás Cabrera", Universidad Autónoma de Madrid, 28049 Madrid, Spain
[c] Condensed Matter Physics Center (IFIMAC), Universidad Autónoma de Madrid, 28049 Madrid, Spain
[d] Instituto Madrileño de Estudios Avanzados en, Nanociencia (IMDEA-Nanociencia), 28049 Madrid, Spain

ARTICLE INFO

Article history:
Received 19 November 2015
Accepted 14 December 2015
Available online 20 December 2015

ABSTRACT

The structure and the low-energy phonon dispersion of graphene (Gr) on Ni(111) have been experimentally investigated with helium atom scattering (HAS). The Rayleigh mode observed for Gr/Ni(111) is almost identical to the one measured on clean Ni(111). The energy of the flexural ZA mode at the $\overline{\Gamma}$ point was found to be ~20 meV, significantly lower than the value predicted by recent DFT calculations. The HAS diffraction spectra reveal that the graphene layer has a three-fold symmetry, with a lattice constant $a = (2.48 \pm 0.02)$ Å and shows an effective step-defect scattering reduction when the Ni(111) is covered with a graphene sheet. Gr/Ni(111) surface is a very efficient and inert mirror for He atoms, with a specular reflectivity of ca. 20%. The predominant role of inelastic scattering in Gr/Ni(111) is revealed by analysis of the diffraction spectra background and Debye–Waller measurements.

1. Introduction

Surface phonon dispersion curves are quite sensitive to interatomic forces of adsorbed layers, including the adlayer–substrate interaction. In the case of graphene (Gr) adlayers, phonon spectra can provide valuable information on the Gr–substrate bond strength, the Gr bending rigidity and the existence of Kohn anomalies. This is especially interesting in systems with a strong Gr–substrate interaction, like Gr/Ni(111), where the Raman signal is suppressed due to strong hybridization of the carbon bands with the substrate. The Gr/Ni(111) system is a very good example of how changes in the strength of the graphene–substrate interaction modify the corresponding phonon dispersion curves [1]. This system is characterized by graphite–like phonon modes, which are softened due to the Gr–substrate interaction [2,3]. This softening is removed after intercalation of Ag or Cu underneath the Gr layer, rendering surface phonon modes which look quite similar to those of graphite [4,5].

In addition, and owing to its low misfit, Gr forms a (1×1) structure on Ni(111) [6]. Therefore, it provides an excellent scenario to test state–of–the–art calculations of surface phonon dispersion curves, which are more difficult to perform in systems where Gr forms moiré superlattices, like Gr/Ir(111), Gr/Pt(111) or Ru(0001) [7–12]. In a recent study, Allard and Wirtz reported LDA–phonon calculations for Gr/Ni(111) [13]. They obtained good agreement with previous HREELS data [2,14], including the softening of the ZO mode and the suppression of the Kohn anomaly at $\overline{\Gamma}$ and $\overline{K}$. However, the data available so far were limited to phonon energies above 40 meV, and therefore did not allow testing the performance of the calculations in reproducing the low–energy acoustical modes. In case of strong Gr–substrate interaction, for instance, hybridization of the low–energy Gr flexural mode with the Rayleigh wave of the substrate is expected to occur, as reported for Gr/TaC(111) [15] and Gr/Ru(0001) [16].

The low–energy acoustic phonon dispersion modes of graphene fall in the range easily accessible to Helium Atom Scattering (HAS). Because of the low energies employed (10–100 meV), neutral He atoms probe the topmost surface layer of any material in an inert, completely non–destructive manner [17]. In this paper, we present a HAS study of the structure and phonon dynamics of the Gr/Ni(111) system. Inelastic HAS spectra are characterized by a comparatively strong intensity from the Ni(111) Rayleigh wave (RW). This is quite surprising, since Ni atoms are completely screened out by the Gr sheet. This helps to explain the high specular reflectivity observed (ca. 20%) to He atoms, suggesting the use of Gr/Ni(111) as a focusing mirror in scanning He atom microscopy [18–20].

* Corresponding author. Departamento de Física de la Materia Condensada, Universidad Autónoma de Madrid, 28049 Madrid, Spain.
E-mail address: daniel.farias@uam.es (D. Farías).

http://dx.doi.org/10.1016/j.carbon.2015.12.043
0008-6223/

2. Experimental

The experiments were performed with a high resolution He atom scattering (HAS) time–of–flight (TOF) spectrometer, described in detail elsewhere [21,22]. Essentially, the He atom beam, produced in a high pressure free jet expansion of the gas, is modulated by a rotating disk chopper for TOF measurements. The helium atoms scattered from the sample, after travelling trough three differentially pumped stages along the 1.7 m long drift tube, are detected by means of a mass sensitive detector. The angle between incident and scattered beam, in a planar geometry, is fixed at a total angle $\theta_{SD} = \theta_i + \theta_f = 105.4^\circ$. The angular distributions are measured by rotating the crystal by angle steps of $\Delta\theta_i = 0.04^\circ$ around a normal to the plane defined by the incident and the outgoing beams. For the thermal attenuation (Debye–Waller) measurements reported in next section a second HAS system has been also used. This apparatus enables determination of absolute diffraction reflectivities by measuring directly the incident beam intensity [23]. In both HAS machines, the beam energy can be varied by changing the nozzle temperature. The beam energies used in the current work were between 26 meV and 80 meV, with the corresponding energy spread varying from 2.2% to 5%, respectively.

The Ni(111) simple crystal used in the study is a disk with a diameter of 8 mm and a thickness of 2 mm. The crystal was mounted on the sample holder which can be heated by electronic bombardment or cooled to 100 K using liquid nitrogen. Sample temperature was measured with a C type thermocouple spot welded to the sample edge. Clean Ni(111) surfaces were prepared in UHV by repeated cycles of ion sputtering (1.5 KeV $P_{Ar} \simeq 1 \times 10^{-5}$ mbar) and flash-annealing at ca 1400 K. After the final annealing the sample was cooled down to 750 K and maintained there during exposure to ethylene at a pressure $P_{C_2H_4} = 5 \times 10^{-7}$ mbar for 20 min. The cleanliness and azimuthal alignment of the sample have been monitored by means of the analysis of HAS angular distributions, as well as by low electron energy diffraction (LEED). The inertness of the Gr/Ni(111) surface was checked by monitoring the specular He–intensity while dosing oxygen from the background. Graphene-passivated samples exhibited a constant He–reflectivity, even one week after sample preparation.

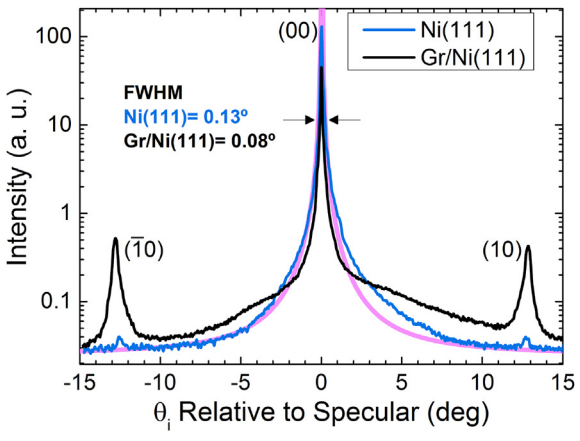

Fig. 1. Angular distribution of He scattering from Ni(111) (blue) and Gr/Ni(111) (black) along the $\overline{\Gamma M}$ direction. The pink curve is a normalized $1/\Delta K^2$ form factor. The incident beam energy is $E_i = 66$ meV and the surface temperature is 100 K. (A colour version of this figure can be viewed online.)

3. Results and discussion

Fig. 1 shows a comparison of He angular distributions from clean Ni(111) and Gr/Ni(111) samples, measured at the same incident beam energy $E_i = 66$ meV and along the $\overline{\Gamma M}$ direction. Sharp diffraction peaks and the high specular intensity indicate the existence of a well-ordered Ni(111) surface and the excellent quality of the graphene monolayer. First order $(\bar{1}\ 0)$ and (10) diffraction peaks are clearly visible from both surfaces; their appearance at the same angular position for both systems confirms the formation of a (1×1) graphene layer. These peaks are an order of magnitude more intense in the case of Gr/Ni(111), indicating a higher surface corrugation. The relative-to-specular intensity of the first order diffraction peaks I_{01}/I_{00} is 1.4% for Gr/Ni(111) and 0.02% for bare Ni(111). Fitting these values using eikonal approximation gives the corrugation values 0.07 Å and 0.009 Å for Gr/Ni(111) and Ni(111), respectively. These corrugations agree well with the recently published [24] 0.06 Å and 0.005 Å for Gr/Ni(111) and Ni(111), respectively. The measured surface corrugation by HAS follows a surface of constant total electron density at the classical turning point of the He atoms [17] which, in turn, is a function of the He kinetic energy [25]. In other words, He atoms with higher energies can take a closer look at the surface where the charge density is more corrugated. This can explain the slightly smaller corrugation values obtained using a He beam with energy 8meV [24] compared to our data using 66meV. The angular position of the diffraction peaks corresponds to a lattice constant $a = (2.48 \pm 0.02)$ Å for Gr/Ni(111). This means that graphene is stretched by ca. 1.6% compared to the value (2.44±0.02) obtained also by HAS for Gr/Cu(111) [26] and by 0.8% compared to the periodicity of a single carbon layer in graphite measured by x-ray diffraction 2.46 Å [27,28]. The specular reflectivity of Gr/Ni(111) compared to the intensity of the directly measured incident He-beam is $I/I_0 = 20\%$ at $T_S = 100$ K, $E_i = 28$ meV and $\theta_i = 60^\circ$, whereas, at the same conditions, the bare Ni(111) reflectivity is 40%.

A quite remarkable result from the comparison of the spectra in Fig. 1 is the observation of a sharper specular peak for the graphene-covered substrate. By performing Gaussian fits to the specular peaks, we obtained peak widths FWHM = 0.13° for Ni(111) and FWHM = 0.08° for Gr/Ni(111). The latter corresponds roughly to the angular resolution of the instrument, revealing the extremely high surface quality of the sample where the graphene sheet softens the step edges of the substrate. The reduced FWHM value obtained for Gr/Ni(111) can be further understood by investigating the different shapes of the background measured from the two samples. The form of the background is determined by inelastic single- and multi–phonon scattering as well as diffuse elastic scattering by defects on the surface.

If the diffuse elastic contribution is from point defects we would expect to see a decay consistent with a $1/\Delta K^3$ envelope, as opposed to a $1/\Delta K^2$ envelope expected for step edges normal to the sagittal scattering plane [29]. The background of the bare Ni(111) surface fits well an envelope of $1/\Delta K^2$, indicating the importance of scattering from step edges in the broadening of the specular peak. On the other hand, the background of Gr/Ni(111) does not fit any of these forms, but rather has a shifted Gaussian shape, which is well explained by inelastic multi–phonon scattering. To better illustrate this effect we compare in Fig. 2 different angular distributions from Gr/Ni(111) with different scattering conditions. When helium atoms with a high incident energy ("hot particles") hit a "cold surface" as in the blue AD, they lose energy on average and thus the background is higher on the energy loss side which is the phonon creation direction ($\Delta K = k_i(\sin(\theta_f) - \sin(\theta_i)) > 0$). Contrarily, when cold particles hit a hot surface (green AD) they gain energy on average and the background is shifted to $\Delta K < 0$. Otherwise, cold

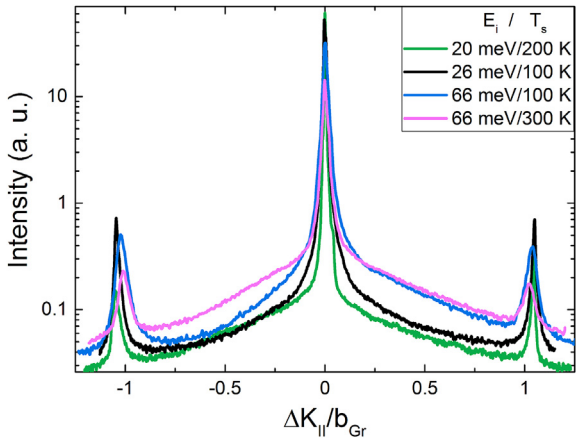

Fig. 2. Angular distributions of He scattering from Gr/Ni(111) for different beam energies and surface temperatures. The horizontal axis has been normalized using Bragg condition to give the change of parallel momentum $\Delta\mathbf{K}_{||}(\text{Å}^{-1})$ relative to the reciprocal lattice vector of graphene $\mathbf{b}_{Gr}(\text{Å}^{-1})$ to normalize the positions of diffraction peaks from measurements with different incident energy E_i. (A colour version of this figure can be viewed online.)

particles hitting a cold surface and hot particles hitting a hot surface (black and pink ADs) lose and gain energy with similar probabilities and the background is more symmetric relative to the specular peak [30,31]. This also can be noticed in the small asymmetry of the background of the clean Ni(111) spectrum shown in Fig. 1. In conclusion, the graphene layer on Ni(111) reduces elastic scattering from step edges, while the lower surface mass results in increasing the inelastic scattering through the Debye-Waller factor.

Fig. 3 shows the structure of the (1 × 1) graphene layer on Ni(111) proposed by Gamo et al. [6] on the basis of LEED I–V measurements. According to this model, a C atom (A) sits on top of a Ni atom, and a second C atom (B) occupies a three-fold fcc hollow site in Fig. 3a–b. These two inequivalent C atoms have a different distance from the 1st Ni-layer Δd = 0.05 Å [6]. DFT calculations for the Gr–Ni(111) bonding [32] showed that there is an electron transfer of ~0.14 electrons per unit cell from Ni(111) to graphene and that only the C atoms located directly above surface Ni atoms accumulate electrons. This indicates that the two C atoms in the graphene unit cell are not only topologically unequivalent, they also have different electronic densities in their vicinities. Although the fcc(111) surface and graphene both have six–fold symmetry, the different positioning and interaction of the C atoms with the Ni atoms results in a triangular rather than hexagonal surface and the overall symmetry is reduced from C_6 to C_3. However, in principle it is not clear if this small asymmetry could be detected by HAS, as the He atoms are scattered by the surface electrons where their density is of the order of 10^{-4} a.u. about 3 Å far from the topmost ion cores [17].

Fig. 3d presents angular distributions recorded along the [$\bar{1}\bar{1}$2] (blue) and [$\bar{2}$11] (black) high symmetry directions, equivalent to $\overline{\Gamma M}$ in the reciprocal space shown in Fig. 3c. The different intensities observed for the first order diffraction peaks in each spectrum prove that, even at the low densities sampled by He atoms, the Gr/Ni(111) surface exhibits a three–fold symmetry. This asymmetry in the measurements is not a result of bad azimuthal alignment of the Ni(111) crystal, as could sometime be the case. In fact, for each spectrum shown in Fig. 3d the azimuthal orientation has been adjusted to maximize the diffraction peak with the lowest intensity even though this resulted in lowering the intensity of the

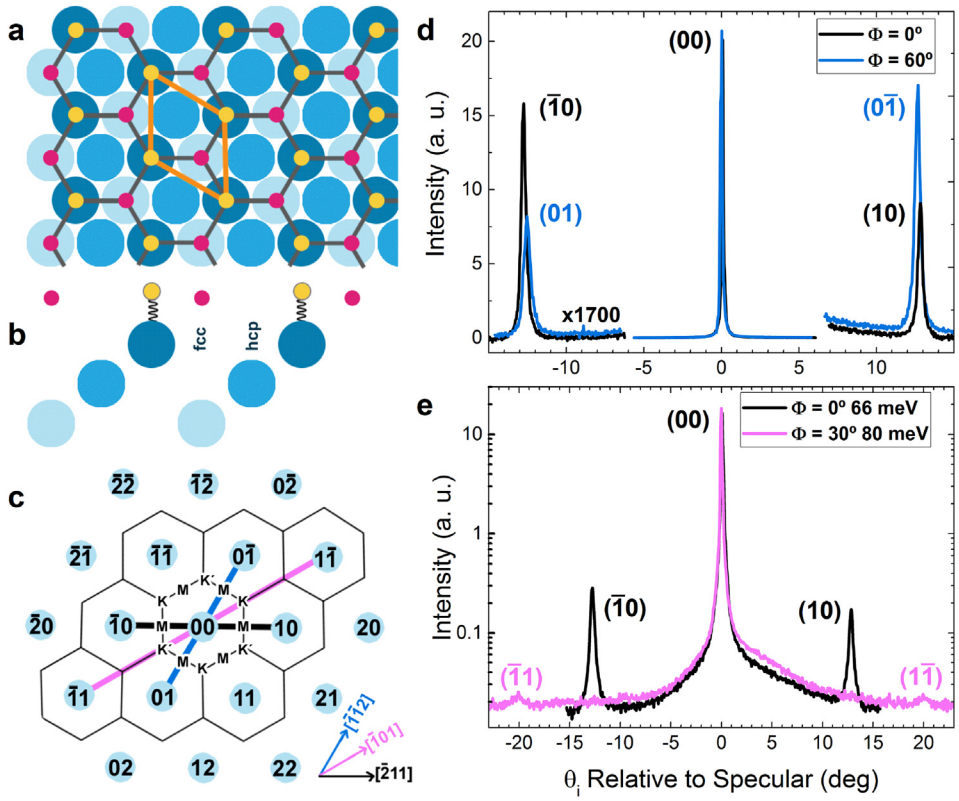

Fig. 3. Top view (a) and side view (b) of real and (c) reciprocal crystalline structure formed by graphene on Ni(111). Red and yellow circles correspond to the inequivalent carbon atoms of the two sublattices. The equal unit cell of Gr and Ni(111) is indicated by orange. (d–e) Angular distribution of He scattering from Gr/Ni(111) along the two main high symmetry directions, the spectrum colors correspond to the color of directions in c. The surface temperature is 120 K. (A colour version of this figure can be viewed online.)

other diffraction peak. Fig. 3e reproduces measurements performed along [$\bar{1}$01], where the second order diffraction peaks ($\bar{1}$1) and (1$\bar{1}$) are detected. This confirms the larger corrugation of Gr/Ni(111) as compared to clean Ni(111) as well as the good quality of its long range crystalline order.

More insight about graphene's interaction with the substrate can be gained from measurements of the thermal attenuation of the specular reflectivity, where the intensity of the reflected beam $I(T)$ is related to the incident beam intensity I_0 by the Debye-Waller (DW) factor [17]:

$$ln(I(T)/I_0) = -2W(T) = -\frac{24m(E_i\cos^2\theta_i + D)T}{Mk_B\Theta_D^2} \quad (1)$$

where m and M are the atomic masses of the projectile and surface, respectively, E_i and θ_i are the incident energy and angle of the beam, k_B is the Boltzmann constant, T is the surface temperature, D is the well-depth of the projectile-surface potential and Θ_D is the Debye-temperature. Fig. 4a shows the thermal attenuation of He specular intensity as a function of surface temperature for Gr/Ni(111), Gr/Cu(111) [26] and Gr/Ru(0001) [33]. Previous and current data except closed blue circles have been measured using the same HAS system [23] which allows measuring the incident beam intensity and thus the absolute reflectivity. The blue closed circles were measured by the HAS-TOF spectrometer and the reflected intensity was normalized by the absolute reflectivity measured in the other HAS system at the same experimental conditions (ca. 20%). By assigning the mass of one carbon atom to the atomic mass of the surface, and D = 15.7 meV to the surface attractive potential well [34], we get a value of the Debye-temperature Θ_D = (687 ± 12) K, which is intermediate between Θ_D = 1045 K for Gr/Ru(0001) [33] and Θ_D = 412 K for Gr/Cu(111) [26]. On the other hand, using the surface effective mass M_{eff} = 6 C reported for He scattering from graphite [35], reduced Θ_D values are obtained, as shown in Table 1.

Determination of the effective surface mass M_{eff} and the surface Debye temperature Θ_D is still a matter of debate in rare–gas atom scattering [36]. For instance, an increased effective mass was used to fit Ar and N_2 scattering data from the Ru(0001) surface, whereas this effect was not observed in other metal surfaces. This was

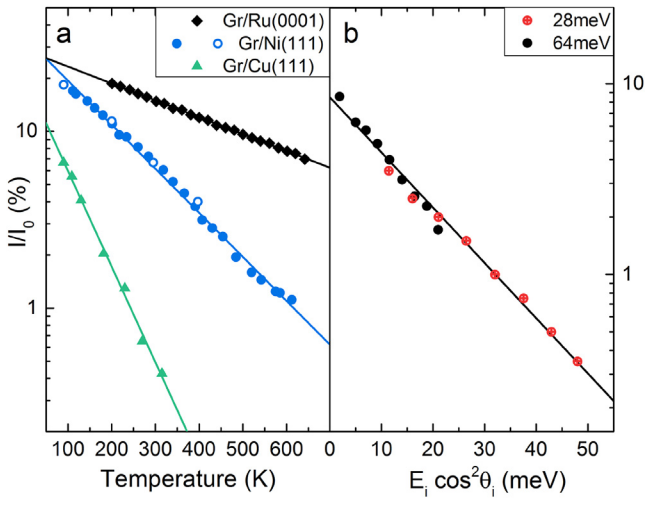

Fig. 4. (a) Thermal attenuation of He–specular intensity for Gr/Cu(111) [26] (E_i = 28 meV, θ_i = 60°) (green triangles), Gr/Ru(0001) [33] (E_i = 32 meV,θ_i = 60°) (black diamonds) and Gr/Ni(111) (E_i = 36.6 meV,θ_i = 52.7°) (open and closed blue circles). (b) He–specular intensity dependence versus incident normal energy for Gr/Ni(111). The data correspond to two different incident energies and a surface temperature T_s = 120 K. (A colour version of this figure can be viewed online.)

Table 1
Debye-Temperature values in K for Gr/metals, calculated using a surface effective mass of 1 or 6C atoms.

System	Θ_D(1C)	Θ_D(6C)
Gr/Ru(0001)	1045 ± 25[33], 1130 ± 50[7]	408
Gr/Ni(111)	687 ± 12, 784 ± 14[24]	280
Gr/Cu(111)	412 ± 10	168

interpreted as due to the different layer stacking (fcc or hcp) of the metallic surfaces investigated, whereby the mass increase in the case of Ru(0001) is caused by Ru atoms in layers beneath the surface [37]. Ar scattering from Gr/Ru(0001) has also shown that an increased M_{eff} is sensed by the scattered atoms [7]. The measured M_{eff} values are 230 and 281 amu for Ru(0001) and Gr/Ru(0001), respectively. The higher M_{eff} of graphene covered metals (mass loading effect) also explains the softening of the RW branch of Gr/Ru(0001) [16]. Additionally, the surface Debye temperature obtained by HAS involves only the out–of–plane acoustic phonon modes, since the optical phonons contribution is assumed to be zero in the Debye model [30,38]. If we assume a mass loading effect in Gr/Ni(111) similar to that observed in Gr/Ru(0001), which is reasonable due to the similar, strong graphene–metal interaction in both systems [9], then M_{eff} is equal to 6 carbon atoms and 1 nickel atom, i.e. 131 amu. The choice of 6C atoms has been attributed to the stiffness of the C–C bond; in HOPG, the measured value is M_{eff} = 72 amu [35]. It has been suggested that Debye–Waller attenuation measurements can be used as a probe of the graphene–substrate interaction [7]. However, using the value of Θ_D derived by using the effective mass of 1 carbon atom one can deduce that the out-of-plane lattice vibration of Gr/Ru(0001) are quite different from those of Gr/Ni(111). This is not the case, however, as proved by the phonon dispersion curves presented below. The difference in the DW factor $2W(T)$ can thus be explained by considering a difference in the effective mass of the surface which appears in the DW factor multiplied to Θ_D. A smaller effective mass allows for a more efficient momentum and energy transfer from the impinging atoms to the surface, reducing its specular reflectivity. Fig. 4b shows He–specular scattering data as a function of incident normal energy, measured at a fixed surface temperature T_s = 120 K and two different incident energies E_i = 28 and 64 meV. The two data sets exhibit quite similar slopes when represented in a log scale, indicating that He–scattering from Gr/Ni(111) obeys normal energy scaling, as expected from a low–corrugated surface.

Fig. 5 shows representative time-of-flight (TOF) spectra converted to energy transfer scale taken at different incident conditions along the $\bar{\Gamma}\bar{M}$ and $\bar{\Gamma}\bar{K}$ directions, for Gr/Ni(111) and bare Ni(111). Each spectrum has been fitted with multiple Gaussian peaks. The diffuse elastic peak (shaded blue) has been taken as the zero in the energy transfer scale. Multi–phonon peaks (grey) appear as broad features that dominate the energy exchange between He-atoms and the studies surfaces. Peaks corresponding to the different phonon modes are labeled: Rayleigh Wave (RW), Longitudinal Resonances (LR) and out–of–plane acoustic mode (ZA). Each peak indicates a phonon energy, the corresponding phonon wave vector is calculated from a scan curve that gives ΔK as a function of ΔE and the other experimental parameters [39]. Scan curves are shown by black solid lines in each panel of Fig. 5. The vertical axes show the values of the momentum transfer corresponding to each scan curve; the intensities of the TOF spectra are not shown as they are usually normalized for calculations. The shape of the diffuse elastic peak is an indicator of the energy spread of the He-beam. The width of this peak increases from 1 to 4 meV when increasing the beam energy from 34 to 80 meV, so clearly a lower incident energy is the best choice for resolving phonon

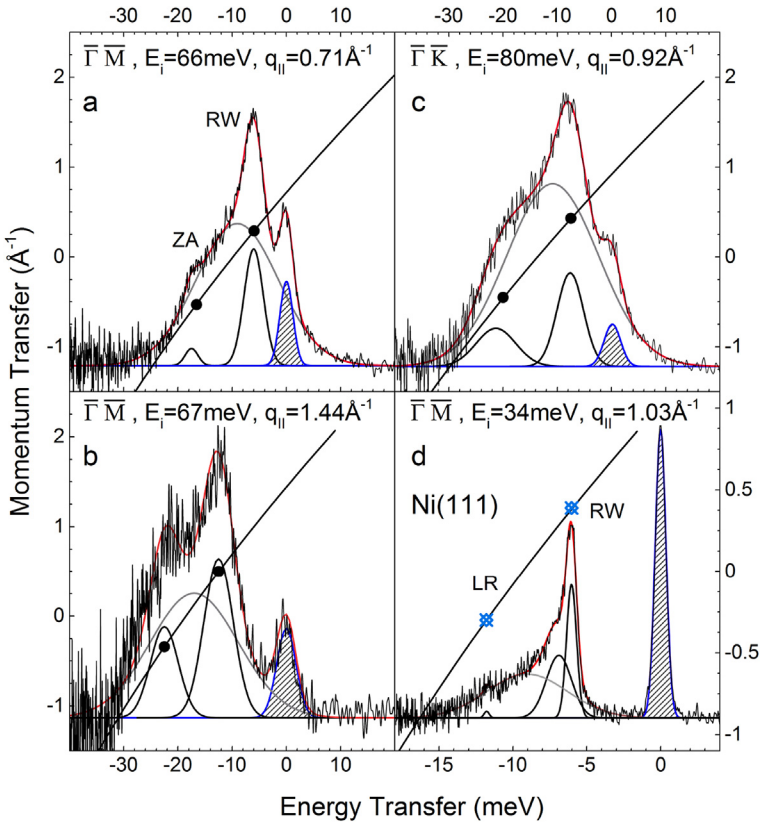

Fig. 5. Selected TOF spectra converted into energy exchange scale for Gr/Ni(111) (a, b and c) and bare Ni(111) (d); the intensity scale of the TOF spectra is not shown. TOF spectra were fitted by multiple Gaussian peaks: diffuse elastic (blue shaded) and broad multi–phonon peak (grey); the other peaks indicate phonon energy losses. Solid black lines represent scan curves; the corresponding momentum transfer ΔK can be read from the vertical scale. Data points extracted from these spectra are indicated for Gr/Ni(111) (black circles) and for Ni(111) (crossed blue diamonds). (A colour version of this figure can be viewed online.)

modes with small energy differences, but a higher energy is required to avoid the HAS intensity cutoff at large energy transfers [40]. The intensity of the diffuse elastic peak decreases for higher beam energies while the intensity of the multi–phonon peak increases; therefore, up to 6 h of data accumulation were required for these measurements. Series of TOF spectra have been recorded under different incident angles for various values of the incident energy, ranging from 34 to 80 meV, and the surface temperature (from 120 K to 400 K), in order to explore the acoustic phonon dispersion curves of Gr/Ni(111) along the two main symmetry

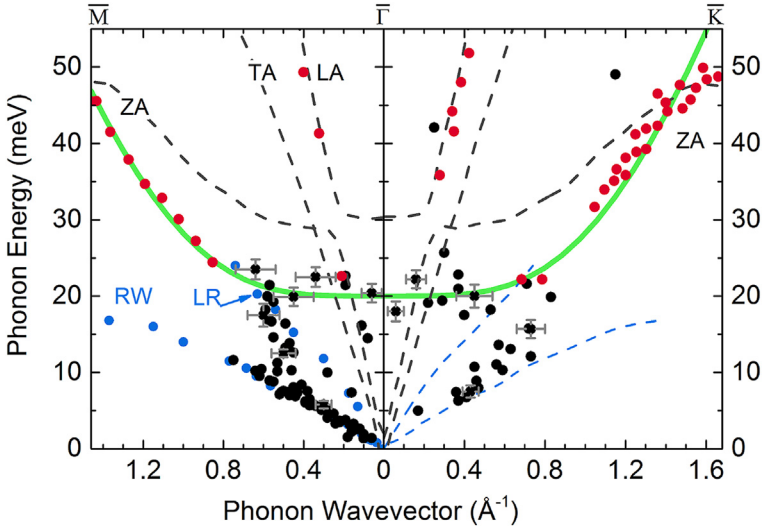

Fig. 6. Surface phonon dispersion of Gr/Ni(111) along the $\overline{\Gamma M}$ and $\overline{\Gamma K}$ directions. Black circles are current low–energy data for Gr/Ni(111). Red circles: HREELS data from Refs. [2,14]. Dashed grey lines are *ab initio* calculations of the Gr/Ni(111) modes [13]. Blue circles are measured data of Ni(111) surface phonon dispersion in $\overline{\Gamma M}$, which are mirrored as dashed lines along $\overline{\Gamma K}$ for visual comparison. (A colour version of this figure can be viewed online.)

direction. TOF spectra presented in Fig. 5a–c show two clear peaks: the largest corresponds to the RW mode of the substrate, while the smallest one belongs to the ZA mode of the graphene layer. The dominant feature observed in the TOF spectra of clean Ni(111) corresponds to the RW mode; the LR mode was usually very hard to detect since its energy falls in the bulk modes' energy band. In some cases, a peak originated in the bulk edge could be detected, as the one close to the RW peak in Fig. 5d.

In this work, we have measured the low–energy part of the dispersion curves of the acoustic phonon modes for Gr/Ni(111) in the $\overline{\Gamma M}$ and $\overline{\Gamma K}$ directions of the surface Brillouin zone (SBZ) and the phonon dispersion of bare Ni(111) along $\overline{\Gamma M}$. Fig. 6 shows the measured data as black circles for Gr/Ni(111) and blue circles for Ni(111); LR and RW dispersion have been determined experimentally and mirrored to the $\overline{\Gamma K}$ direction as blue dashed lines for visual comparison. For completeness, we have also included the low–energy data measured by HREELS along $\overline{\Gamma M}$ [14] and $\overline{\Gamma K}$ [2] (red circles) as well as results reported by *ab initio* calculations (dashed lines) [13].

The most pronounced feature in the measured phonon dispersion is the presence of the same RW of Ni(111) up to half the SBZ in the $\overline{\Gamma M}$ direction, where it undergoes a hybridization with the LR mode. No hybridization between LR and RW modes was observed for the bare Ni(111) surface. Also, a few data points of the LR mode have also been detected in the Gr/Ni(111) measurements. Since the He-phonon interaction is directly related to the electron–phonon coupling strength [41] and due to the strong C–Ni bonding, it is not surprising to detect the RW mode of the metallic substrate as has been the case for Gr/Ru(0001) [16], although, unlike the latter no data points of RW of Gr/Ni(111) could be measured in the second half of the SBZ due to the momentum cutoff for out-of-plane vibrations at large wave vectors, and thus no information on the mass loading effect could be obtained from the phonon dispersion. Even more surprising is the different behavior of RW along the $\overline{\Gamma K}$ direction, where the data points appear at slightly higher energies. We note that the sagittal plane is not a mirror symmetry plane for the atomic displacements of the Shear Horizontal (SH) mode of Ni(111) in the $\overline{\Gamma K}$ direction, and thus the coupling to the impinging He-atoms' momentum to this mode is not forbidden by symmetry. Only two data points corresponding to the LA mode have been resolved along $\overline{\Gamma M}$, while in the $\overline{\Gamma K}$ direction the large scattering of the data points at ca. 20 meV near $\overline{\Gamma}$ could be a result of the avoided crossing of the LA and ZA modes. Well–resolved peaks were not obtained because the elastic scattering is dominated by the multi–phonon scattering. The few resolved data points are in good agreement with the dispersion curves measured by HREELS and calculated for LA mode of Gr/Ni(111).

The major difference between Gr/Ni(111) and graphene concerns the ZA branch, which does not go to zero for $\Delta K \rightarrow 0$ due to the symmetry breaking induced by the Gr–Ni interplanar force constants. Our data along the two symmetry directions, considering also previously reported HREELS data [14,2], gives an energy of ~20meV for the ZA mode at the $\overline{\Gamma}$ point. This is close to the 16meV reported for Gr/Ru(0001) [16], but it is much lower than the 30meV reported by recent LDA–phonon calculations [13]. The dispersion of the ZA mode can be fitted (as shown by the green solid line in Fig. 6) using [42]:

$$\omega_{ZA}^{coupled}(\Delta K) = \sqrt{\frac{\kappa}{\rho_{2D}}\Delta K^4 + \omega_0^2}, \quad (2)$$

where $\omega_0 = g/\rho_{2D}$, $\rho = 7.6 \times 10^{-8}$ g/cm^2 is the two-dimensional mass density of graphene; g is the coupling strength between graphene and the substrate and κ is the bending rigidity of the graphene sheet. Fitting Eq. (2) to our data gives $g = (7.15 \pm 0.7) \times 10^{20}$ N/m^3 and $\kappa = (0.43 \pm 0.07)$ eV. These values can be compared with the ones obtained for Gr/Cu(111) also with HAS [26]: $g = (0.57 \pm 0.04) \times 10^{20}$ N/m^3 and $\kappa = (1.30 \pm 0.15)$ eV. It is clear that the graphene–Ni coupling is much stronger, and that the graphene bending rigidity is reduced as a consequence of being forced to follow the surface vibrations of the Ni atoms.

It is worth pointing out that the DFT calculations reported in Ref. [13] of Gr/Ni(111) provide a good description of the optical phonon branches, including the softening of the ZO mode and the suppression of the Kohn anomaly observed by HREELS [2,14] along $\overline{\Gamma M}$. Actually, from the overestimation of the ZA/ZO gap at $\overline{\Gamma}$ and $\overline{K}$ the authors of Ref. [13] concluded that their LDA calculations may be overestimating the adsorption strength of graphene on the Ni substrate. Our current results seem to confirm this view. Finally, the fact that the lowest observed branch on Gr/Ni(111) is actually the substrate RW accounts for the observed high specular reflectivity (ca. 20%) to He atoms, and confirms that systems with a strong C–substrate interaction are the best candidates to be used as focusing mirrors in scanning He atom microscopy.

4. Conclusions

We have presented a helium atom scattering study of the structure and acoustic phonon modes of graphene on Ni(111). The lattice constant of graphene on Ni(111) determined from He–diffraction spectra is $a = (2.48 \pm 0.02)$ Å. A quite surprising result is the observation of essentially the same Rayleigh mode on both clean Ni(111) and Gr/Ni(111) surfaces. This is interpreted as due to the strong C–Ni bonding, which allows graphene to closely follow the vibrations of the substrate Ni atoms. This finding provides an explanation for the high specular reflectivity (ca. 20%) of Gr/Ni(111) to He atoms, suggesting its use as inert focusing mirror in scanning He atom microscopy [18]. Finally, the energy of the ZA mode at the $\overline{\Gamma}$ point was found to be ~20 meV, well below the 30 meV reported by recent DFT calculations [13]. It is hoped that the present results will stimulate more accurate calculations of the phonon dynamics of Gr/Ni(111).

Acknowledgements

We gratefully acknowledge J.P. Toennies and the Max-Planck-Gesellschaft for the donation of the scattering apparatus used in our experiments. We are grateful to Prof. J.R. Manson and Prof. G. Benedek for their insightful comments. This work has been supported by the European Union, FP7: Theme NMP.2012.1.4–3 Grant no. 309672, and by projects FIS 2013-40667-P and FrontNano-Magnet (S-2013/MIT-3007) from the Comunidad de Madrid.

References

[1] C. Oshima, A. Nagashima, Ultra-thin epitaxial films of graphite and hexagonal boron nitride on solid surfaces, J. Phys. Condens. Matter 9 (1) (1997) 1.
[2] A.M. Shikin, D. Farías, V.K. Adamchuk, K.H. Rieder, Surface phonon dispersion of a graphite monolayer adsorbed on Ni(111) and its modification caused by intercalation of Yb, La and Cu layers, Surf. Sci. 424 (1999) 155.
[3] D. Farías, K.H. Rieder, A.M. Shikin, V.K. Adamchuk, T. Tanaka, C. Oshima, Modification of the surface phonon dispersion of a graphite monolayer adsorbed on Ni(111) caused by intercalation of Yb, Cu and Ag, Surf. Sci. 454–456 (1) (2000) 437.
[4] A.M. Shikin, D. Farías, K.H. Rieder, Phonon stiffening induced by copper intercalation in monolayer graphite on Ni(111), Europhys. Lett. 44 (1) (1998) 44.
[5] D. Farías, A.M. Shikin, K.H. Rieder, Y.S. Dedkov, Synthesis of a weakly bonded graphite monolayer on Ni(111) by intercalation of silver, J. Phys. Condens. Matter 11 (43) (1999) 8453.
[6] Y. Gamo, A. Nagashima, M. Wakabayashi, M. Terai, C. Oshima, Atomic structure of monolayer graphite formed on Ni(111), Surf. Sci. 374 (1–3) (1997) 61.
[7] H. Shichibe, Y. Satake, K. Watanabe, A. Kinjyo, A. Kunihara, Y. Yamada, M. Sasaki, W.W. Hayes, J.R. Manson, Probing interlayer interactions between

graphene and metal substrates by supersonic rare-gas atom scattering, Phys. Rev. B 91 (15) (2015) 155403.
[8] J. Wintterlin, M.L. Bocquet, Graphene on metal surfaces, Surf. Sci. 603 (10–12) (2009) 1841.
[9] M. Batzill, The surface science of graphene: metal interfaces, CVD synthesis, nanoribbons, chemical modifications, and defects, Surf. Sci. Rep. 67 (3–4) (2012) 83.
[10] A.T. N'Diaye, J. Coraux, T.N. Plasa, C. Busse, T. Michely, Structure of epitaxial graphene on Ir(111), New J. Phys. 10 (4) (2008) 043033.
[11] A.L. Vázquez de Parga, F. Calleja, B. Borca, M.C.G. Passeggi, J.J. Hinarejos, F. Guinea, R. Miranda, Periodically rippled graphene: growth and spatially resolved electronic structure, Phys. Rev. Lett. 100 (2008) 056807.
[12] B. Borca, S. Barja, M. Garnica, D. Sánchez-Portal, V.M. Silkin, E.V. Chulkov, C.F. Hermanns, J.J. Hinarejos, A.L. Vázquez de Parga, A. Arnau, P.M. Echenique, R. Miranda, Potential energy landscape for hot electrons in periodically nanostructured graphene, Phys. Rev. Lett. 105 (2010) 036804.
[13] A. Allard, L. Wirtz, Graphene on metallic substrates: suppression of the Kohn Anomalies in the phonon dispersion, Nano Lett. 10 (11) (2010) 4335.
[14] T. Aizawa, R. Souda, Y. Ishizawa, H. Hirano, T. Yamada, K. Tanaka, C. Oshima, Phonon dispersion in monolayer graphite formed on Ni(111) and Ni(001), Surf. Sci. 237 (1–3) (1990) 194.
[15] T. Aizawa, R. Souda, S. Otani, Y. Ishizawa, C. Oshima, Bond softening in monolayer graphite formed on transition-metal carbide surfaces, Phys. Rev. B 42 (18) (1990) 11469.
[16] D. Maccariello, D. Campi, A. Al Taleb, G. Benedek, D. Farías, M. Bernasconi, R. Miranda, Low-energy excitations of graphene on Ru(0001), Carbon 93 (2015) 1.
[17] D. Farías, K.H. Rieder, Atomic beam diffraction from solid surfaces, Rep. Prog. Phys. 61 (12) (1998) 1575.
[18] B. Holst, W. Allison, An atom-focusing mirror, Nature 390 (6657) (1997) 244.
[19] K. Fladischer, et al., An ellipsoidal mirror for focusing neutral atomic and molecular beams, New J. Phys. 12 (2010) 033018.
[20] D. Barredo, F. Calleja, P. Nieto, J.J. Hinarejos, G. Laurent, A.L. Vázquez de Parga, D. Farías, R. Miranda, A quantum–stabilized mirror for atoms, Adv. Mater. 20 (2008) 3492.
[21] H.J. Ernst, E. Hulpke, J.P. Toennies, Helium-atom-scattering study of the structure and phonon dynamics of the W(001) surface between 200 and 1900 K, Phys. Rev. B 46 (24) (1992) 16081.
[22] D. Barredo, G. Laurent, P. Nieto, D. Farías, R. Miranda, High-resolution elastic and rotationally inelastic diffraction of D2 from NiAl(110), J. Chem. Phys. 133 (12) (2010) 124702.
[23] P. Nieto, D. Barredo, D. Farías, R. Miranda, In-plane and out-of-plane diffraction of H2 from Ru(001), J. Phys. Chem. A 115 (25) (2011) 7283.
[24] A. Tamtögl, E. Bahn, J. Zhu, P. Fouquet, J. Ellis, W. Allison, Graphene on Ni(111): electronic corrugation and dynamics from helium atom scattering, J. Phys. Chem. C 119 (46) (2015) 25983–25990 (available online).
[25] M.I. Trioni, G. Fratesi, S. Achilli, G.P. Brivio, Dynamics of electron distributions probed by helium scattering, J. Phys. Condens. Matter 21 (26) (2009) 264003.
[26] A. Al Taleb, H.K. Yu, G. Anemone, D. Farías, A. Wodtke, Helium diffraction and acoustic phonons of graphene grown on copper foil, Carbon 95 (2015) 731.
[27] J.B. Nelson, D.P. Riley, The thermal expansion of graphite from 15° C. to 800° C.: part I. experimental, Proc. Phys. Soc. 57 (6) (1945) 477.
[28] M. Mohr, J. Maultzsch, E. Dobardžić, S. Reich, I. Milošević, M. Damnjanović, A. Bosak, M. Krisch, C. Thomsen, Phonon dispersion of graphite by inelastic x-ray scattering, Phys. Rev. B 76 (3) (2007) 035439.
[29] F. Hofmann, J.P. Toennies, J.R. Manson, A comprehensive experimental study of the dynamical interaction of He atoms with Cu(001) surface phonons, J. Chem. Phys. 101 (11) (1994) 10155.
[30] J.R. Manson, Multiphonon atom-surface scattering, Comput. Phys. Commun. 80 (1–3) (1994) 145.
[31] W.W. Hayes, J.R. Manson, Classical and semiclassical theories of atom scattering from corrugated surfaces, Phys. Rev. B 89 (4) (2014) 045406.
[32] S.M. Kozlov, F. Viñes, A. Görling, Bonding mechanisms of graphene on metal surfaces, J. Phys. Chem. C 116 (13) (2012) 7360.
[33] A. Politano, B. Borca, M. Minniti, J.J. Hinarejos, A. Vázquez de Parga, D. Farías, R. Miranda, Helium reflectivity and debye temperature of graphene grown epitaxially on Ru(0001), Phys. Rev. B 84 (3) (2011) 23.
[34] G. Boato, P. Cantini, C. Salvo, R. Tatarek, S. Terreni, Atomic vibrations at the (0001) graphite surface studied by He atom scattering, Surf. Sci. 14 (1982) 485.
[35] J.P. Oh, T. Kondo, D. Hatake, J. Nakamura, Elastic and inelastic scattering components in the angular intensity distribution of He scattered from graphite, Surf. Sci. 603 (6) (2009) 895.
[36] W.W. Hayes, J.R. Manson, Argon scattering from Ru(0001): calculations and comparison with experiment, Phys. Rev. B 75 (2007) 113408.
[37] W.W. Hayes, H. Ambaye, J.R. Manson, Atomic and molecular collisions with surfaces: Comparisons of Ar and N2 scattering from Ru(0001), J. Phys. Condens. Matter 19 (2007) 305007.
[38] A. Cocemasov, D.L. Nika, A. Balandin, Engineering of the thermodynamic properties of bilayer graphene by atomic plane rotations: the role of the out-of-plane phonons, Nanoscale 7 (30) (2015) 12851.
[39] D.M. Smilgies, J.P. Toennies, Resolution and intensity considerations of an ideal He atom time-of-flight spectrometer for measurements of surface phonon dispersion curves, Rev. Sci. Instrum. 59 (10) (1988) 2185.
[40] G. Benedek, M. Bernasconi, V. Chis, E. Chulkov, P.M. Echenique, B. Hellsing, J.P. Toennies, Theory of surface phonons at metal surfaces: recent advances, J. Phys. Condens. Matter 22 (8) (2010) 084020.
[41] G. Benedek, M. Bernasconi, K. Bohnen, D. Campi, E.V. Chulkov, P.M. Echenique, R. Heid, I. Yu Sklyadneva, J.P. Toennies, Unveiling mode-selected electron-phonon interactions in metal films by helium atom scattering, Phys. Chem. Chem. Phys. 16 (16) (2014) 7159.
[42] B. Amorim, F. Guinea, Flexural mode of graphene on a substrate, Phys. Rev. B 88 (11) (2013) 115418.